ACS OMEGA

http://pubs.acs.org/journal/acsodf

Article

Fabrication of Efficient Electrocatalysts for Electrochemical Water Oxidation Using Bimetallic Oxides System

Abid Ali, Dure Najaf, Arif Nazir,* Ali Haider, Munawar Iqbal, Norah Alwadai, Abida Kausar, and Azhar Ahmad

Cite This: *ACS Omega* 2023, 8, 9539−9546

Read Online

ACCESS | Metrics & More | Article Recommendations

ABSTRACT: The study focused on the fabrication of nickel, cobalt, and their bimetallic oxide via a facile electrodeposition approach over the surface of conducting glass has been reported here. Fabricated electrodes have been employed as binder-free and effective anode materials toward oxygen evolution reactions (OER) in electrochemical water splitting at high pH. Nickel and cobalt oxides showed overpotential values of 520 mV and 536 mV at the current density of 10 $mAcm^{-2}$ with charge transfer resistances of 170 and 195 Ω. For bimetallic oxides (NiCoO@FTO), the overpotential depressed up to 460 mV and lower charge transfer value of 80 Ω. Additionally, double-layer capacitance also boosted for the bimetallic oxide with a value of 199 μF as compared to monometallic nickel oxide (106 μF) and cobalt oxide (120 μF). Multimetal oxides of Ni−Co showed the best performance, which was further supported with larger electrochemical surface area. This facile approach toward the electrode fabrication could be a charming alternate to replace the Ru- and Ir-based expensive materials for OER in electrochemical water splitting.

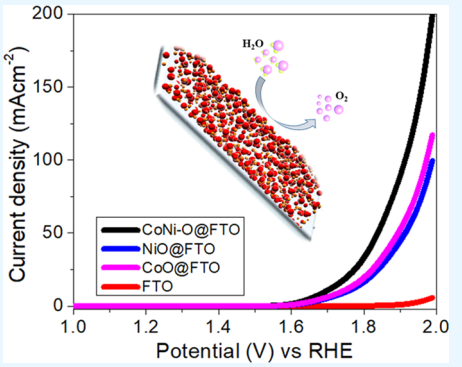

1. INTRODUCTION

Energy is crucial for the development of society, the global economy, and nonrenewable fossil fuels. Currently, resources are meeting 65% of global energy demands. Fossil fuels release harmful greenhouse gases like CO_2, which cause global warming and other environmental problems.[1−5] To combat the depletion of fossil fuels and the rise in CO_2 emissions, at least 10 terawatt-hour (TWh) of renewable energy must be produced by 2050. This energy can come from sources like solar, wind, hydroelectricity, biomass, ocean thermal, and sea waves/tides.[6−8]

Research into renewable energy sources must go hand in hand with the development of energy storage technology. Electrochemical technology, one of numerous potential energy storage techniques, is currently the most feasible and effective way to store and transform renewable energy. Electrochemical technologies include batteries, electrolysis, compressed air, flywheels, pumped hydroelectricity, and magnetic superconductors.[9−12] The most effective way to store energy among the numerous electrochemical energy technologies currently in use is to electrolyze water in order to produce hydrogen (H_2). The development of water electrolysis technology for the production of H_2 is therefore of great importance. Hydrogen, as a green fuel, has a substantial potential to fulfill the energy demand along with the reduction of greenhouse gases. However, during water electrolysis, oxygen evolution reaction (OER) has a sluggish kinetics with four electron transfers at the electrode surface. To facilitate the OER at the anode, transition metal-based oxide as electrode material has significant potential with superior catalytic activity.[13−16]

Electrochemical water splitting currently attains enough consideration due to less solar utilization proficiency for water electrolysis in the photoelectrochemical process. Electrochemical splitting of water comprises two half-reactions, the hydrogen evolution reaction (HER) at the cathode side and the oxygen evolution reaction (OER) at the anode. Usage of extraordinary HER and OER electrocatalyst is a good impetus for increasing the rate of water splitting, which leads to minimizing the overpotential value.[17−19]

Ru and Ir are the universal noble metals that are used for water splitting because of their greater stability and smaller overpotential rate, whereas Pd and Pt can also be useful but their activity toward water splitting is lesser than that of Ir and Ru. The increasing activity order for the water splitting process is illustrated here: Pd < Pt < Ir < Ru. Though Ru certifies higher activity, the poor stability of Ru prohibits it from functional use in comparison to other electrocatalysts. Moreover, in electrochemical reactions, porous materials have various advantages for

Received: December 31, 2022
Accepted: February 21, 2023
Published: March 3, 2023

https://doi.org/10.1021/acsomega.2c08288
ACS Omega 2023, 8, 9539−9546

charge transference due to their extraordinary high surface area. The immobilization of these metal NPs such as Ir, Ru, Au, Ag, RuO_2, and IrO_2 on carbonaceous surface is an efficient solution to this report dilemma, as scientists have acknowledged that NPs offer good activity with respect to electrocatalysis as to their total counterparts.[20,21]

Various earth abundant transition metals (TMs) like Fe-, Ni-, and Co-based electrocatalysts for the HER and OER show greater performance. Recently, these low-cost electrocatalytic substances have been reported, and some of them present superior electrochemical water splitting efficiency. These nonprecious metals paid significant role for the progression and improvement of energy material due to their easy availability, extraordinary activity earth abundance. Due to the presence of 3d electrons, their variable oxidation states, and structural properties, the transition metal compounds are favorable as well in OER catalyst applications. Furthermore, by changing their microstructures, surface area, and particle size, the efficiency of these compounds can be further improved.[22]

An enormous amount of earth-rich transition metal-based catalysts comprising transition metal oxides, hydroxide, phosphides, sulfides, nitrides, and multiple elements doped transition metal electrocatalysts are well-known bifunctional catalysts that are used in overall electrochemical splitting of water because of their cheap, high electrocatalytic performances and earth abundance. Higher HER and OER activity depiction by these bifunctional electrocatalysts has been synthesized by various facile methods. Mixed valence transition metal oxides such as $FeCo_2O_4$, $CoMn_2O_4$, and $NiCo_2O_4$, with their spinel organization, have higher electrocatalytic performance due to their higher conductivity, excellent morphological stability, and abundant oxidation states.[23,24]

A catalyst with shell nanoarray configuration on nickel foam (NF) was invented by Zhang et al., wherein thin layer of $CoNiO_2$ was covered as a shell on NiCo essential for TWS. In alkaline medium for OER and HER, the rate of current density was reported to be 10 $mAcm^{-2}$ by overpotential of 320 and 156 mV, correspondingly. Moreover, once it was used as both anode and cathode, 1.688 voltage was achieved to deliver 10 mA cm^{-2} current.[25] So, to increase the electrocatalytic activity and active sites, it is very effective for electrocatalyst immobilization on a conductive substrate. According to Xu et al.,[22] for TWS, on the carbon nanotubes (CNTs), the immobilized $NiFe_2O_4$ nanohybrid marked as $NiFe_2O_4$/CNT by supercritical carbon dioxide methodology showed high activity in alkaline medium for HER and OER with overpotential of 0.15 and 0.24 V at a current density of 0.01 $mAcm^{-2}$, respectively. For the TWS, this increasing activity referred to collaboration of CNTs and $NiFe_2O_4$ nanohybrid, which provided enormous active sites, high diffusion rate of reactants, and charge mobility. Therefore, it is shown that to reduce the lower electrical conductance and higher charge mobility and expose active sites, transition metal oxides are normally immobilized and associated on a conductive support to formulate the hybrid catalyst for TWS.[26]

Amorphization is unique, effective, and superficial trick that contains short-range ordering and atomic defects in catalytic substances. As compared to crystalline catalysts, amorphous catalysts are novel because of their defect richness, chemical homogeneity, and structural flexibility at an atomic level. Recently, numerous amorphous phase catalysts have been reported, which revealed superior performance for electrolysis for TWS for both HER and OER in almost all types of electrocatalysis medium.[27−29]

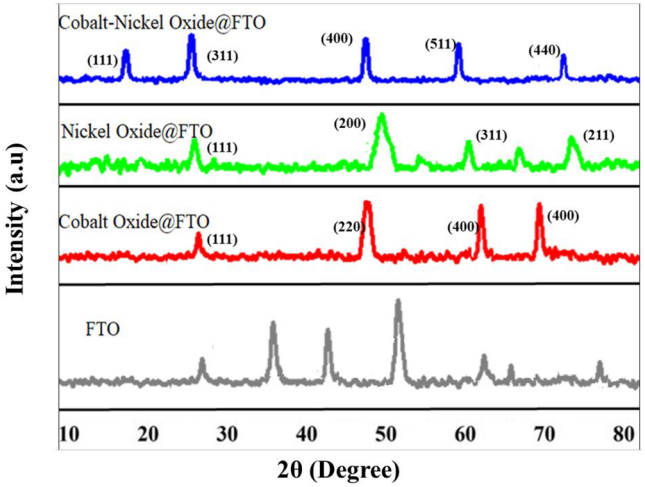

Figure 1. XRD patterns of bare FTO, Co−O@FTO, Ni−O@FTO, and NiCoO@FTO.

To immobilize the electrocatalysts on a supportive material, electrodeposition is a highly favorable method. Mixed metal oxides of variable composition could be deposited on an electrode surface in a superficial technique through this method. So, metal oxides that are electrochemically immobilized do not face insulation assets of binding materials and hold a greater interaction with the helpful and conductive electrodes, which in turn improves their electrocatalytic activity with greater stability and high density of current with high evolution kinetics of gas.[30−32]

The fabrication of amorphous materials with high surface roughness and surface area for higher electrocatalytic activity can be done easily, economically, and environmentally through the use of electrodeposition. Its binder-free method, which has more stickiness to the substrate and higher activity, is another advantage of electrodeposition over other methods used for the synthesis of these materials.[33−35]

In this study, we fabricated amorphous cobalt oxide (CoO@FTO), nickel oxide (NiO@FTO), and their bimetallic oxide (NiCoO@FTO) by electrochemical deposition followed by annealing. NiCoO@FTO demonstrated improved electrocatalytic characteristics in comparison to the other produced oxides based on polarization curves, Tafel slopes, and electrochemical impedance tests. Additionally, supporting this were NiCoO@FTO showing higher electrochemical double-layer capacitance (C_{dl}) and higher electrochemical surface area (ECSA), which offered more active sites for the electron-transfer process. Nyquist plots with smaller semicircle diameter reflect NiCoO@FTO demonstrating lower charge-transfer resistance. Chronoamperometry tests showed that all electrodes that had been made were stable when tested for the continuous production of oxygen for 10 h.

2. MATERIALS AND METHODS

An electrodeposition approach has been adopted for the fabrication of the mono and bimetallic oxides of transition metal (Ni, Co) over the surface of conducting glass (FTO). Deionized water and ethanol were used for the cleaning of FTO under sonication. Cobalt(II) chloride hexa-hydrate (99.9%) and nickel(II) sulfate hexa-hydrate (99.9%) were attained from Sigma-Aldrich. Analytical-grade potassium hydroxide, sulfuric acid, and boric acid were purchased from Alfa Aesar. FTO glass

https://doi.org/10.1021/acsomega.2c08288
ACS Omega 2023, 8, 9539−9546

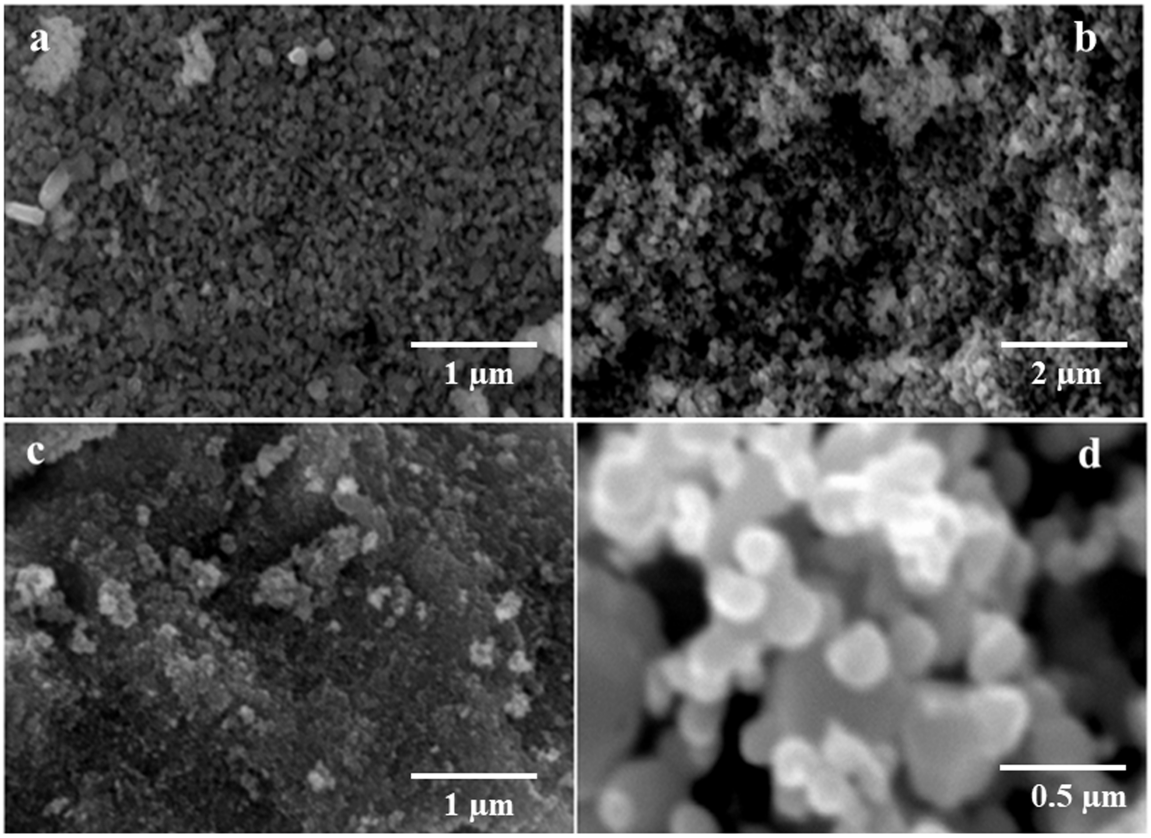

Figure 2. SEM images of (a) Ni−O@FTO, (b) Co−O@FTO, and (c) NiCoO@FTO lower and (d) high NiCoO@FTO resolution illustrating the morphology.

Table 1. Comparison of Electrocatalytic OER Performance of Different Amorphous Materials

catalyst as anode	electrolyte	η @ 10 mAcm^{-2}	ref
amorphous $Co(OH)_2$ nanosheets	0.1 M KOH	380	39
amorphous $CoVO_x$	1 M KOH	347	40
amorphous IrOx	1 M H_2SO_4	220	41
amorphous $Fe_6Ni_{10}O_x$	1 M KOH	286	42
amorphous $Ni_{0.69}Fe_{0.31}O_x$	1 M KOH	280	43
amorphous Ni−Co binary oxide	1 M NaOH	325	44
amorphous Ni−Fe oxides/carbon nanohybrid	0.1 M KOH	290	45
amorphous Ni−Fe hydroxide	1 M KOH	189	46
Co_3N@amorphous N-doped Carbon	1 M KOH	280	47
Amorphous $Co_{0.63}Fe_{0.21}P_{0.16}$	1 M KOH	217	48
amorphous Co_2−Fe-B	1 M KOH	298	49
amorphous Cu−Ni−Fe	1 M KOH	224	50
CoNi-O@FTO	1 M KOH	460	this study

(TEC 15, Hartford Glass Co., 15 Ω/square, 50 × 13 × 2.3 mm^3), isopropyl alcohol, and acetone were bought commercially.

2.1. Preparation of Fluorine-Doped Tin Oxide. FTO-based substrate was cleaned in deionized water and acetone twice under ultrasonication. First, it was sonicated in the cleanser solution for 10 min. After cleaning with deionized water, FTO glass was rinsed with acetone for 15 min. Then the substrate was cleaned in hot deionized water followed by drying in air.

2.2. Electrodeposition of Metal Oxides on FTO-Coated Glass. FTO glass, 1 × 1 cm^2, used as a substrate for the electrodeposition of mono and bimetallic oxide of nickel and cobalt. One-third of the conducting substrate was carried outside the deposition bath and hanged with the conducting clipper while voltage was applied. Chronoamperometric method was used at the fixed potential of −1.1 V for a period of 60 s. The electrodeposition was performed in a three-electrode cell comprising an equimolar electrolytic solution of corresponding salts of metals in existence of boric acid. H_2SO_4 was used to maintain the pH of prepared solution at 3. The samples that had been deposited were immediately washed with deionized water to remove all of the unreacted components and annealed for 2 h at 350 °C in air with a heating rate of 0.5 °C per minute.

2.3. Electrochemical Measurements. The electrochemical experimentation was accomplished in a three-electrode cell in alkaline media (1 M KOH). The working electrode was FTO (1 × 1 cm^2), whereas platinum wire was used as a counter electrode and saturated Ag/AgCl as a reference electrode. A Gamry interface 1010e potentiostat/Galvanostat was used to measure all electrochemical parameters. The measured potentials throughout the experiments were transformed with respect to reversible hydrogen electrode (RHE) using the following pH-dependent mathematical formulation:

$$E_{RHE} = E_{Ag/AgCl} + 0.197 + 0.059 \quad (1)$$

When plot overpotential (η) versus log(j) and then Tafel plots were attained, Tafel plot linear fragments were suited to the equation of Tafel:

$$\eta = b \log(j) + a \quad (2)$$

https://doi.org/10.1021/acsomega.2c08288
ACS Omega 2023, 8, 9539−9546

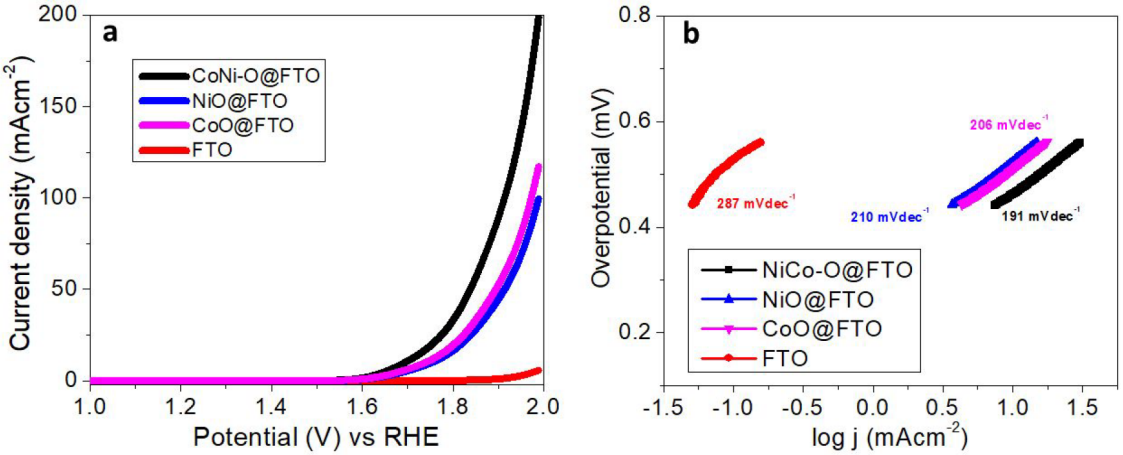

Figure 3. (a) Polarization curves for the electrodeposited CoO@FTO, NiO@FTO, and NiCoO@FTO electrodes in 1 M KOH aqueous solution at a scan rate of 5 mV s^{-1} and (b) their corresponding Tafel plots obtained from the polarization curves.

in which "a" is exchange current density, "b" is Tafel slope, and "*j*" is current density. A frequency of 100 kHz to 0.1 Hz has been applied by a minor AC signal of 10 mV for the electrochemical impedance measurements. Chronoamperometry technique was used to verify the stability of the fabricated electrodes, whereas gradually producing oxygen in 1 M aqueous solution of KOH was performed on a continuous potential equivalent to 10 $mAcm^{-2}$ of respective electrocatalyst.[36,37]

3. RESULTS AND DISCUSSION

Mono and bimetallic oxides-based electrodes were formed by electrodeposition on FTO. In the initial stage, we have made binary- and monometal oxides of cobalt and nickel owing to their famous activity for water splitting. Through several techniques, the manufactured materials were characterized and then more electrochemical activity was examined. For the characterization of electrochemically deposited materials, two techniques were used: the first one is scanning electron microscopy (SEM) to define the materials morphologies and then powder X-ray diffraction (XRD) spectroscopy to find out the phase.

3.1. Powder X-ray Diffraction Analysis. To examine the amorphous structural identity, modified FTO samples were analyzed via powder XRD. The lack of any high-pitched peaks for the deposited films over FTO surface indicated that the electrodeposited transition metal-based oxides catalysts are primarily X-ray amorphous. Figure 1 represents the XRD patterns for unmodified FTO glass and CoO@FTO, NiO@FTO, and NiCoO@FTO associated with the position SnO_2 JCPDS. The broader peaks associated with nickel, cobalt, and their bimetallic oxide might be due to the low crystallinity of the deposited materials or the existence of tiny grains occupying the interspaces among the particles. Similar peaks in the range of 28°, 50°, and 60° obtained for bimetallic oxide, grown in the (111), (220), and (411) orientation, confirmed the mixed mode of both nickel and cobalt in the XRD pattern of fabricated materials.

3.2. Morphology of Material. Scanning electron microscopy (SEM) analysis was further performed to evaluate the morphology of the as-prepared electrode materials. SEM images for Ni−O@FTO, Co−O@FTO, and NiCoO@FTO are shown in Figure 2. NiO@FTO pictures (Figure 2a) illustrated the rough distribution of its spherical particles, whereas in case of Co−O@FTO (shown in Figure 2b), owing to particles accumulation, no clear shape was detected. Figure 2d further showed an in-depth analysis of the bimetallic oxide (NiCoO@FTO) with a mixture of irregular rectangular cubes spherical shaped particles. Almost 500 nm particle size elaborated for the mixture of the nickel- and cobalt-based bimetallic oxides.

3.3. Electrochemical Studies. *3.3.1. Linear Sweep Voltammetry.* Electrocatalytic oxygen evolution reaction performance of FTO-based mono and binary-metal oxide electrodes (containing Ni and Co) was observed in basic solution (1 M KOH) by using an ordinary three-electrode system (Table 1). Linear sweep voltammetry was used for the electrochemical verification of synthesized electrodes at a potential range of 0−2.0 V against reversible hydrogen electrode (RHE) at a scan rate of 5 mV s^{-1}. Figure 3a represents bare FTO polarization curves and their comparison behavior with the mono and bimetallic oxides of transition metals over the FTO surface.

Overpotential values for the electrocatalysts CoO@FTO and NiO@FTO were observed to be 536 and 520 mV, respectively, at the current density of 10 $mAcm^{-2}$. For the higher current value of 100 $mAcm^{-2}$, the required overpotential was increased to 990 mV for CoO@FTO and 890 mV for NiO@FTO. Related to these monometal oxide electrodes, the overpotential for binary-metal oxide (NiCoO@FTO) was expressively reduced to 460 mV at 10 $mAcm^{-2}$ and 745 mV at 100 $mAcm^{-2}$. This reduction in overpotential shown by binary-metal oxide electrode verified its higher electrocatalytic OER performance as compared to both monometal oxide electrodes.

Tafel slope is inversely related to charge transfer ability, which indicates that a good catalyst has a small Tafel slope. In Figure 3b, the Tafel slope of modified electrodes along with bare FTO, generated from the polarization curves, was used to further analyze the electrochemical performance in terms of OER kinetics. Tafel slope considerations from the Tafel plots were to be ∼210 mV dec^{-1} and ∼206 mV dec^{-1} for CoO@FTO and NiO@FTO, respectively. In comparison with NiCoO@FTO, which showed the lowest value of Tafel slope, that is, 191 mV dec^{-1}. This lower slope represented that the unification of Co and Ni binary-metal increased the electrocatalytic performance with high promising kinetics toward OER. This might be recognized by a greater number of active sites and surface area

https://doi.org/10.1021/acsomega.2c08288
ACS Omega 2023, 8, 9539−9546

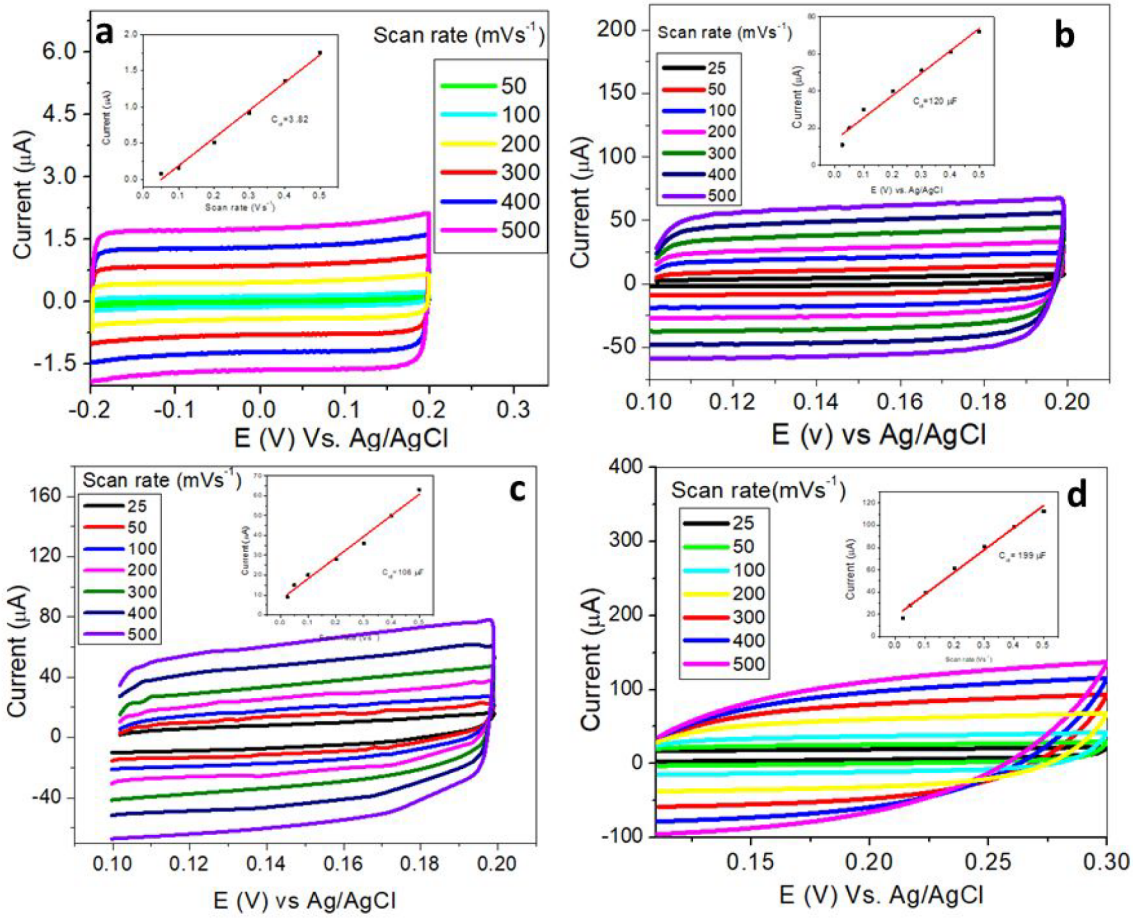

Figure 4. (a) CV curves for bare FTO, the electrodeposited (b) Ni−O@FTO, (c) Co−O@FTO, and (d) NiCoO@FTO electrodes in 1 M KOH aqueous solution at different scan rates, and their corresponding plots for electrochemical double layer capacitance.

owned by NiCoO@FTO rather than monometal oxide-based electrodes as well as synergistic effect of both the metals.[38]

3.3.2. Cyclic Voltammetry. In order to examine the double layer capacitance (C_{dl}) of the electrocatalysts, a relationship between nonfaradaic current amount and scan rate has been studied by cyclic voltammetry. Higher current densities with faster scan rates have been attributed to the enhanced charging current and reduced diffusion-layer resistance. CV was executed in the nonfaradic section at several scan rates to evaluate the C_{dl} and electrochemical surface area (ECSA) for each electrocatalyst. A linear relationship was observed when scan rate was plotted against current (Figure 4a−d). NiCoO@FTO in 1 M KOH electrolyte exhibited the highest nonfaradaic current (potential window of 0.1 to 0.2 V) and showed the C_{dl} value of 199 μF as shown in Figure 4d. In comparison with the mono metallic nickel and cobalt oxide-based electrocatalysts, they showed C_{dl} values of 120 and 106 as shown in Figure 4b and c, respectively. At the electrode−electrolyte interface, C_{dl} is an essential parameter that is also associated with the ECSA of the electrode material. The greater is the ECSA and higher the double-layer capacitance, consequently the better is electrocatalytic performance toward the OER in water splitting reactions. In monometallic oxides, ECSA values for CoO@FTO and NiO@FTO are 1.13 cm^2 and 1.21 cm^2, respectively. In evaluation with bimetallic oxide (NiCoO@FTO), ECSA revealed a highest significant improved value of 1.91 cm^2. The higher values of C_{dl} and ECSA can be recognized toward the greater surface area with additional biding sites (defects) and subsequently amplified productivity. Electrochemical parameters for each sample such as overpotential, Tafel slope, ECSA and C_{dl}, and R_{ct} are given in Table 2.

Table 2. Electrochemical Parameters for Co, Ni, and Their Binary-Metal Oxide-Based FTO Electrodes

catalysts	η_{10} (mV)[a]	Tafel slope (mV dec^{-1})	C_{dl} (μF)	ECSA (cm^2)	R_{ct} (Ω)
FTO		287	3.82		
CoO@FTO	536	210	106	1.13	195
NiO@FTO	520	206	120	1.21	170
NiCoO@FTO	460	191	199	1.91	80

[a]Where η_{10} is the overpotential at current density of 10 mAcm^{-2}.

3.4. Post Treatment SEM Analysis. After electrochemical water oxidation in basic media, the structural morphology of the bimetallic oxides (NiCoO@FTO) was examined. Figure 5 shows the post analyzed morphology of the metal oxide-coated FTO with (a) lower and (b) higher magnification. The amorphous structure active sites have been blocked up to a small extent with the −OH ions interaction and reduced its activity with the passage of time, which also is shown by the chronoamperometric studies.

3.5. Electrochemical Impedance Spectroscopy and Chronoamperometry. Electrochemical impedance spectroscopy (EIS) was used to examined the charge transfer behavior of

https://doi.org/10.1021/acsomega.2c08288
ACS Omega 2023, 8, 9539−9546

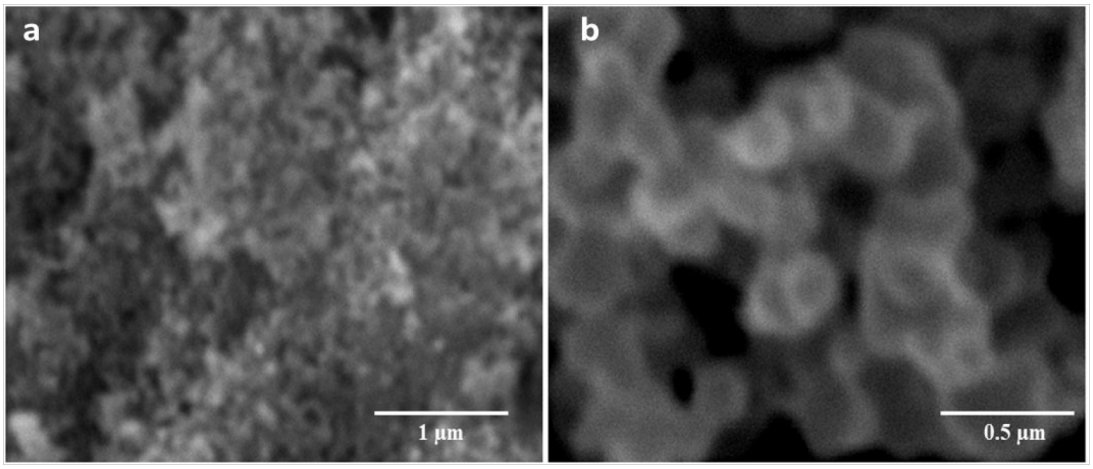

Figure 5. SEM images of NiCoO@FTO at (a) lower and (b) higher resolution illustrating the morphology.

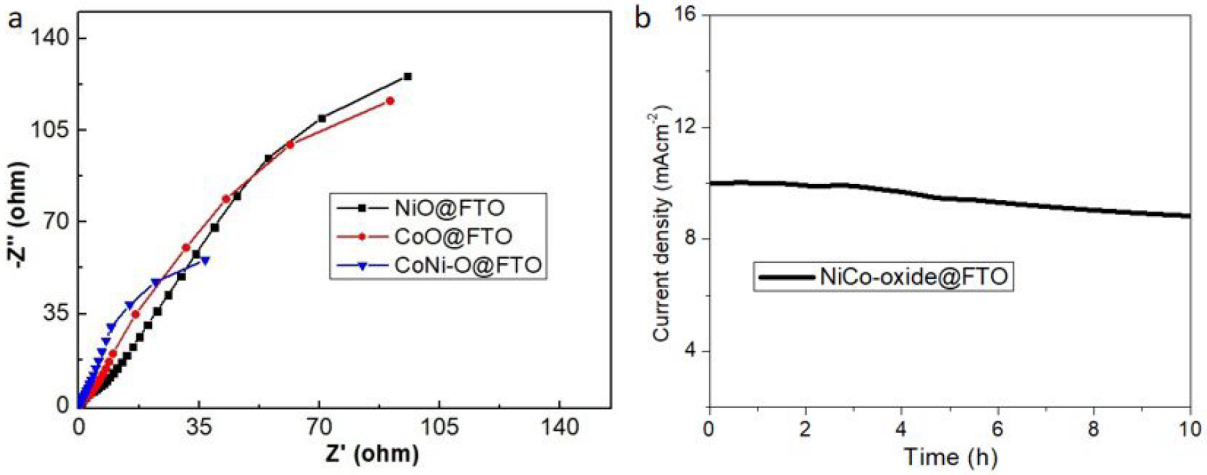

Figure 6. (a) Electrochemical impedance spectroscopy measurements as of 0.1 Hz to 100 kHz for the electrodeposited CoO@FTO, NiO@FTO, and NiCoO@FTO electrodes at a DC voltage of 0.7 V. (b) Chronoamperometry for the electrode stability at a fixed potential of 0.65 V.

the oxygen evolution reaction activity for different electrodes as shown in Figure 6a. The real part of resistance has been plotted against its imaginary portion in the Nyquist plot. Semicircle thickness in the higher frequency region displays the resistance of charge-transfer for electrocatalysts and depicts the kinetics of electron transfer of on the interface (electrode−electrolyte). As compared to both CoO@FTO and NiO@FTO electrodes, NiCoO@FTO showed a smaller semicircle, which represented lower charge transfer resistance values of 195 Ω, 170 Ω, and 80 Ω, respectively. Solution resistance values of all electrode systems showed the same position at the real part of the Nyquist plot. The results therefore showed a quicker electron-transfer process occur at the electrode composed of binary-metal oxide to enhance the OER process.

The electrode stability is also a crucial parameter to assess the durability and performance of the electrocatalyst in the electrochemical water splitting process. The fabricated electrode stability was verified by using the chronoamperometry technique while progressively producing oxygen in 1 M KOH aqueous solution at a continuous potential equivalent to 10 mA cm^{-2} for NiCoO@FTO for 10 h. Figure 6b shows the stability consequence for FTO-based electrodes modified with binary-metal oxides. Electrocatalysts exhibited good stability in amperometric quantities, showing the durability of the fabricated amorphous electrocatalysts toward OER at a current density of 10 $mAcm^{-2}$, representing a good candidate for the electrocatalytic water oxidation reaction.[51]

4. CONCLUSIONS

An electrodeposited approach has been adopted for the oxides of Ni, Co, and their bimetallic for the efficient oxygen evolution reaction in electrochemical water splitting. Linear sweep voltammetry, cyclic voltammetry, and electrochemical impedance spectroscopy were used to study the electrochemical behavior of the metals and multimetal oxides. Bimetallic oxide of Ni and Co showed the best performance with lowest overpotential of 460 mV as compared to NiO@FTO (520 mV) and CoO@FTO (536 mV). Amorphous structure oxides exhibited better stability when examined by chronoamperometry for 10 h. Double-layer capacitance and charge transfer resistance also revealed that the oxide of the bimetallic presented efficient electrocatalytic activities toward OER in electrochemical water splitting reactions.

https://doi.org/10.1021/acsomega.2c08288
ACS Omega 2023, 8, 9539−9546

AUTHOR INFORMATION

Corresponding Author

Arif Nazir − *Department of Chemistry, The University of Lahore, Lahore 54590, Pakistan;* orcid.org/0000-0002-9412-6100; Email: anmalik77@gmail.com

Authors

Abid Ali − *Department of Chemistry, The University of Lahore, Lahore 54590, Pakistan;* orcid.org/0000-0002-0452-4827

Dure Najaf − *Department of Chemistry, The University of Lahore, Lahore 54590, Pakistan*

Ali Haider − *Department of Chemistry, Quaid-i-Azam University, Islamabad 45320, Pakistan;* orcid.org/0000-0001-8755-2454

Munawar Iqbal − *Department of Chemistry, Division of Science and Technology, University of Education, Lahore 54770, Pakistan*

Norah Alwadai − *Department of Physics, College of Sciences, Princess Nourah bint Abdulrahman University, Riyadh 11671, Saudi Arabia*

Abida Kausar − *Department of Chemistry, Government College Women University Faisalabad, Faisalabad 38000, Pakistan*

Azhar Ahmad − *Department of Chemistry, The University of Lahore, Lahore 54590, Pakistan*

Complete contact information is available at: https://pubs.acs.org/10.1021/acsomega.2c08288

Notes

The authors declare no competing financial interest.

ACKNOWLEDGMENTS

The authors express their gratitude to Princess Nourah bint Abdulrahman University Researchers Supporting Project number (PNURSP2023R11), Princess Nourah bint Abdulrahman University, Riyadh, Saudi Arabia. We are gratified to the HEC for financial support under the startup research Grant No. 21-2146/SRGP/R&D/HEC/2018. The authors are also highly thankful to Prof. Huisheng Peng at the Laboratory of Advance Materials, Fudan University China for providing the CNTs fiber.

REFERENCES

(1) Zhu, J.; Hu, L.; Zhao, P.; Lee, L. Y. S.; Wong, K.-Y. Recent advances in electrocatalytic hydrogen evolution using nanoparticles. *Chem. Rev.* **2020**, *120* (2), 851−918.

(2) Iqbal, M.; Ghaffar, A.; Nazir, A.; Yameen, M.; Munir, B.; Nisar, N.; Bokhari, T. H. Coal desulfurization using gamma and ultraviolet radiation. *Energy Sources, Part A: Recovery, Utilization, and Environmental Effects* **2017**, *39* (11), 1109−1115.

(3) Amjed, N.; Iqbal, M.; Bhatti, I. A.; Nazir, A. Coal desulphurization and conditions optimization through response surface methodology, Khushab mines, Pakistan. *Energy Sources, Part A: Recovery, Utilization, and Environmental Effects* **2017**, *39* (12), 1235−1241.

(4) Korir, K. K.; Benecha, E. M.; Nyamwala, F. O.; Lombardi, E. B. Tuning electronic structure of ZnO nanowires via 3d transition metal dopants for improved photo-electrochemical water splitting: An ab initio study. *Materials Today Communications* **2021**, *26*, 101929.

(5) Wang, Z.; Karaman, E. S.; Meng, X.; Di Benedetto, G.; Zunino, J. L.; Mitra, S. Development of high-capacity flexible sodium manganese periodate batteries with dual polymer electrolytes. *Materials Today Communications* **2021**, *26*, 101928.

(6) Liu, Y.-L.; Yang, C.-L.; Wang, M.-S.; Ma, X.-G.; Yi, Y.-G. Te-doped perovskite NaTaO3 as a promising photocatalytic material for hydrogen production from water splitting driven by visible light. *Mater. Res. Bull.* **2018**, *107*, 125−131.

(7) Nishat, S. S.; Islam, M. T.; Ahmed, S.; Kabir, A. Ab initio study of oxygen evolution reaction and hydrogen evolution reaction via water splitting on pure and nitrogen-doped graphene surface. *Materials Today Communications* **2020**, *25*, 101602.

(8) Singh, A.; Tejasvi, R.; Karmakar, S.; Basu, S. α-Fe2O3 nanorods decorated with NiMnO3 co-catalyst as photoanode for enhanced oxygen evolution reaction in photoelectrochemical water splitting. *Materials Today Communications* **2021**, *27*, 102231.

(9) Shi, Y.; Zhang, B. Recent advances in transition metal phosphide nanomaterials: synthesis and applications in hydrogen evolution reaction. *Chem. Soc. Rev.* **2016**, *45* (6), 1529−1541.

(10) Ao, K.; Wei, Q.; Daoud, W. A. MOF-derived sulfide-based electrocatalyst and scaffold for boosted hydrogen production. *ACS Appl. Mater. Interfaces* **2020**, *12* (30), 33595−33602.

(11) Guo, Y.; Zhou, X.; Tang, J.; Tanaka, S.; Kaneti, Y. V.; Na, J.; Jiang, B.; Yamauchi, Y.; Bando, Y.; Sugahara, Y. Multiscale structural optimization: Highly efficient hollow iron-doped metal sulfide heterostructures as bifunctional electrocatalysts for water splitting. *Nano Energy* **2020**, *75*, 104913.

(12) Guo, Y.; Zhang, C.; Zhang, J.; Dastafkan, K.; Wang, K.; Zhao, C.; Shi, Z. Metal-organic framework-derived bimetallic NiFe selenide electrocatalysts with multiple phases for efficient oxygen evolution reaction. *ACS Sustainable Chem. Eng.* **2021**, *9* (5), 2047−2056.

(13) Sobrino, F. H.; Monroy, C. R.; Pérez, J. L. H. Critical analysis on hydrogen as an alternative to fossil fuels and biofuels for vehicles in Europe. *Renewable and Sustainable Energy Reviews* **2010**, *14* (2), 772−780.

(14) Septiani, N. L. W.; Kaneti, Y. V.; Fathoni, K. B.; Kani, K.; Allah, A. E.; Yuliarto, B.; Nugraha; Dipojono, H. K.; Alothman, Z. A.; Golberg, D.; et al. Self-assembly of two-dimensional bimetallic nickel-cobalt phosphate nanoplates into one-dimensional porous chainlike architecture for efficient oxygen evolution reaction. *Chem. Mater.* **2020**, *32* (16), 7005−7018.

(15) Hu, S.; Wang, S.; Feng, C.; Wu, H.; Zhang, J.; Mei, H. Novel MOF-derived nickel nitride as high-performance bifunctional electrocatalysts for hydrogen evolution and urea oxidation. *ACS Sustainable Chem. Eng.* **2020**, *8* (19), 7414−7422.

(16) Septiani, N. L. W.; Kaneti, Y. V.; Fathoni, K. B.; Guo, Y.; Ide, Y.; Yuliarto, B.; Jiang, X.; Dipojono, H. K.; Golberg, D.; Yamauchi, Y.; et al. Tailorable nanoarchitecturing of bimetallic nickel-cobalt hydrogen phosphate via the self-weaving of nanotubes for efficient oxygen evolution. *Journal of Materials Chemistry A* **2020**, *8* (6), 3035−3047.

(17) Zhou, Y.; Fan, H. J. Progress and challenge of amorphous catalysts for electrochemical water splitting. *ACS Materials Letters* **2021**, *3* (1), 136−147.

(18) Nazir, A.; Khalid, F.; Rehman, S. u.; Sarwar, M.; Iqbal, M.; Yaseen, M.; Iftikhar Khan, M.; Abbas, M. Structural, electric and dielectric properties of perovskite based nanoparticles for energy applications. *Zeitschrift für Physikalische Chemie* **2021**, *235* (6), 769−784.

(19) Naseer, A.; Ali, A.; Ali, S.; Mahmood, A.; Kusuma, H. S.; Nazir, A.; Yaseen, M.; Khan, M. I.; Ghaffar, A.; Abbas, M.; Iqbal, M. Biogenic and eco-benign synthesis of platinum nanoparticles (Pt NPs) using plants aqueous extracts and biological derivatives: environmental, biological and catalytic applications. *Journal of Materials Research and Technology* **2020**, *9* (4), 9093−9107.

(20) Li, H.; Chen, S.; Lin, H.; Xu, X.; Yang, H.; Song, L.; Wang, X. Nickel diselenide ultrathin nanowires decorated with amorphous nickel oxide nanoparticles for enhanced water splitting electrocatalysis. *Small* **2017**, *13* (37), 1701487.

(21) Khaliq, N.; Bibi, I.; Majid, F.; Arshad, M. I.; Ghafoor, A.; Nazeer, Z.; Ezzine, S.; Alwadai, N.; Nazir, A.; Iqbal, M. Mg1-xNixFe2-xCrxO4 synthesis via hydrothermal route: Effect of doping on the structural, optical, electrical, magnetic and photocatalytic properties. *Results in Physics* **2022**, *43*, 106059.

(22) Xu, S.; Lv, C.; He, T.; Huang, Z.; Zhang, C. Amorphous film of cerium doped cobalt oxide as a highly efficient electrocatalyst for

oxygen evolution reaction. *Journal of Materials Chemistry A* **2019**, *7* (13), 7526−7532.
(23) Moni, P.; Hyun, S.; Vignesh, A.; Shanmugam, S. Chrysanthemum flower-like NiCo 2 O 4-nitrogen doped graphene oxide composite: an efficient electrocatalyst for lithium-oxygen and zinc-air batteries. *Chem. Commun.* **2017**, *53* (55), 7836−7839.
(24) Tan, X.; Duan, Z.; Liu, H.; Wu, X.; Cho, Y.-R. Core-shell structured MoS2/Ni9S8 electrocatalysts for high performance hydrogen and oxygen evolution reactions. *Mater. Res. Bull.* **2022**, *146*, 111626.
(25) Zhang, B.; Zhang, X.; Wei, Y.; Xia, L.; Pi, C.; Song, H.; Zheng, Y.; Gao, B.; Fu, J.; Chu, P. K. General synthesis of NiCo alloy nanochain arrays with thin oxide coating: a highly efficient bifunctional electrocatalyst for overall water splitting. *J. Alloys Compd.* **2019**, *797*, 1216−1223.
(26) Li, X.; Wang, Y.; Wang, J.; Da, Y.; Zhang, J.; Li, L.; Zhong, C.; Deng, Y.; Han, X.; Hu, W. Sequential electrodeposition of bifunctional catalytically active structures in MoO3/Ni-NiO composite electrocatalysts for selective hydrogen and oxygen evolution. *Adv. Mater.* **2020**, *32* (39), 2003414.
(27) Liang, H.; Gandi, A. N.; Xia, C.; Hedhili, M. N.; Anjum, D. H.; Schwingenschlogl, U.; Alshareef, H. N. Amorphous NiFe-OH/NiFeP electrocatalyst fabricated at low temperature for water oxidation applications. *ACS Energy Letters* **2017**, *2* (5), 1035−1042.
(28) Han, K.; Dai, P.; Yang, Y.; Wu, M. FeS2/CoS2 nanoparticles supported on N, S co-doped carbon nanotubes as advanced bifunctional electrocatalysts for rechargeable zinc-air batteries. *Mater. Res. Bull.* **2022**, *154*, 111942.
(29) Yang, L.; Ding, H.; Xu, G.; Zhang, L.; Wei, B. Efficient ORR activity of N-doped porous carbon encapsulated cobalt electrocatalyst derived from a novel bimetal-organic framework. *Mater. Res. Bull.* **2021**, *138*, 111237.
(30) Ji, J.; Zhang, L. L.; Ji, H.; Li, Y.; Zhao, X.; Bai, X.; Fan, X.; Zhang, F.; Ruoff, R. S. Nanoporous Ni (OH) 2 thin film on 3D ultrathin-graphite foam for asymmetric supercapacitor. *ACS Nano* **2013**, *7* (7), 6237−6243.
(31) Almessiere, M. A.; Slimani, Y.; Güngüneş, H.; Korkmaz, A. D.; Zubar, T.; Trukhanov, S.; Trukhanov, A.; Manikandan, A.; Alahmari, F.; Baykal, A. Influence of Dy3+ ions on the microstructures and magnetic, electrical, and microwave properties of [Ni0. 4Cu0. 2Zn0. 4](Fe2-x Dy x) O4 (0.00≤ x≤ 0.04) spinel ferrites. *ACS omega* **2021**, *6* (15), 10266−10280.
(32) Alagha, O.; Ouerfelli, N.; Kochkar, H.; Almessiere, M. A.; Slimani, Y.; Manikandan, A.; Baykal, A.; Mostafa, A.; Zubair, M.; Barghouthi, M. H. Kinetic Modeling for Photo-Assisted Penicillin G Degradation of (Mn0. 5Zn0. 5)[CdxFe2-x] O4 (x≤ 0.05) Nanospinel Ferrites. *Nanomaterials* **2021**, *11* (4), 970.
(33) Li, L.; Shao, Q.; Huang, X. Amorphous oxide nanostructures for advanced electrocatalysis. *Chem. Eur. J.* **2020**, *26* (18), 3943−3960.
(34) Manikandan, A.; Yogasundari, M.; Thanrasu, K.; Dinesh, A.; Raja, K. K.; Slimani, Y.; Jaganathan, S. K.; Srinivasan, R.; Baykal, A. Structural, morphological and optical properties of multifunctional magnetic-luminescent ZnO@ Fe3O4 nanocomposite. *Physica E: Low-dimensional Systems and Nanostructures* **2020**, *124*, 114291.
(35) Almessiere, M. A.; Trukhanov, A. V.; Khan, F. A.; Slimani, Y.; Tashkandi, N.; Turchenko, V. A.; Zubar, T. I.; Tishkevich, D. I.; Trukhanov, S. V.; Panina, L. V.; et al. Correlation between microstructure parameters and anti-cancer activity of the [Mn0. 5Zn0. 5](EuxNdxFe2−2x) O4 nanoferrites produced by modified sol-gel and ultrasonic methods. *Ceram. Int.* **2020**, *46* (6), 7346−7354.
(36) Gu, L.; Wang, Y.; Lu, R.; Guan, L.; Peng, X.; Sha, J. Anodic electrodeposition of a porous nickel oxide-hydroxide film on passivated nickel foam for supercapacitors. *Journal of Materials Chemistry A* **2014**, *2* (20), 7161−7164.
(37) Li, Y.; Ai, C.; Deng, S.; Wang, Y.; Tong, X.; Wang, X.; Xia, X.; Tu, J. Nitrogen doped vertical graphene as metal-free electrocatalyst for hydrogen evolution reaction. *Mater. Res. Bull.* **2021**, *134*, 111094.
(38) Nagajyothi, P. C.; Ramaraghavulu, R.; Shim, J. Microwave synthesis: CuCo2O4/CuO as efficient electrocatalysts for the oxygen evolution reaction. *Mater. Lett.* **2023**, *331*, 133449.
(39) Gao, Y. Q.; Li, H. B.; Yang, G. W. Amorphous Co (OH) 2 nanosheet electrocatalyst and the physical mechanism for its high activity and long-term cycle stability. *J. Appl. Phys.* **2016**, *119* (3), 034902.
(40) Shen, F.-C.; Wang, Y.; Tang, Y.-J.; Li, S.-L.; Wang, Y.-R.; Dong, L.-Z.; Li, Y.-F.; Xu, Y.; Lan, Y.-Q. CoV2O6-V2O5 coupled with porous N-doped reduced graphene oxide composite as a highly efficient electrocatalyst for oxygen evolution. *ACS Energy Letters* **2017**, *2* (6), 1327−1333.
(41) Smith, R. D. L.; Sporinova, B.; Fagan, R. D.; Trudel, S.; Berlinguette, C. P. Facile photochemical preparation of amorphous iridium oxide films for water oxidation catalysis. *Chem. Mater.* **2014**, *26* (4), 1654−1659.
(42) Kuai, L.; Geng, J.; Chen, C.; Kan, E.; Liu, Y.; Wang, Q.; Geng, B. A reliable aerosol-spray-assisted approach to produce and optimize amorphous metal oxide catalysts for electrochemical water splitting. *Angew. Chem.* **2014**, *126* (29), 7677−7681.
(43) Qiu, Y.; Xin, L.; Li, W. Electrocatalytic oxygen evolution over supported small amorphous Ni-Fe nanoparticles in alkaline electrolyte. *Langmuir* **2014**, *30* (26), 7893−7901.
(44) Yang, Y.; Fei, H.; Ruan, G.; Xiang, C.; Tour, J. M. Efficient electrocatalytic oxygen evolution on amorphous nickel-cobalt binary oxide nanoporous layers. *ACS Nano* **2014**, *8* (9), 9518−9523.
(45) Chen, G.; Zhu, Y.; Chen, H. M.; Hu, Z.; Hung, S. F.; Ma, N.; Dai, J.; Lin, H. J.; Chen, C. T.; Zhou, W.; et al. An amorphous nickel-iron-based electrocatalyst with unusual local structures for ultrafast oxygen evolution reaction. *Adv. Mater.* **2019**, *31* (28), 1900883.
(46) Li, B.; Chen, S.; Tian, J.; Gong, M.; Xu, H.; Song, L. Amorphous nickel-iron oxides/carbon nanohybrids for an efficient and durable oxygen evolution reaction. *Nano Research* **2017**, *10* (11), 3629−3637.
(47) Kang, B. K.; Im, S. Y.; Lee, J.; Kwag, S. H.; Kwon, S. B.; Tiruneh, S.; Kim, M.-J.; Kim, J. H.; Yang, W. S.; Lim, B.; et al. In-situ formation of MOF derived mesoporous Co3N/amorphous N-doped carbon nanocubes as an efficient electrocatalytic oxygen evolution reaction. *Nano Research* **2019**, *12* (7), 1605−1611.
(48) Wang, T.; Wang, C.; Jin, Y.; Sviripa, A.; Liang, J.; Han, J.; Huang, Y.; Li, Q.; Wu, G. Amorphous Co-Fe-P nanospheres for efficient water oxidation. *Journal of Materials Chemistry A* **2017**, *5* (48), 25378−25384.
(49) Chen, H.; Ouyang, S.; Zhao, M.; Li, Y.; Ye, J. Synergistic activity of Co and Fe in amorphous Co x-Fe-B catalyst for efficient oxygen evolution reaction. *ACS Appl. Mater. Interfaces* **2017**, *9* (46), 40333−40343.
(50) Cai, Z.; Li, L.; Zhang, Y.; Yang, Z.; Yang, J.; Guo, Y.; Guo, L. Amorphous nanocages of Cu-Ni-Fe hydr (oxy) oxide prepared by photocorrosion for highly efficient oxygen evolution. *Angew. Chem.* **2019**, *131* (13), 4233−4238.
(51) Collins, G.; Kasturi, P. R.; Karthik, R.; Shim, J.-J.; Sukanya, R.; Breslin, C. B. Mesoporous carbon-based materials and their applications as non-precious metal electrocatalysts in the oxygen reduction reaction. *Electrochim. Acta* **2023**, *439*, 141678.

https://doi.org/10.1021/acsomega.2c08288
ACS Omega 2023, 8, 9539−9546